Journal of Materials Chemistry A

ROYAL SOCIETY OF CHEMISTRY

PAPER

View Article Online
View Journal | View Issue

Cite this: J. Mater. Chem. A, 2025, 13, 39128

Sustainable materials for organic photovoltaic devices towards transient electronics in digital agriculture

Beata Synkiewicz-Musialska, *[a] Kaisa-Leena Väisänen, [b] Marja Välimäki, *[b] Kiranmai Uppuluri, [a] Maria Smolander, [c] Krzysztof Szostak [a] and Liisa Hakola [c]

With the growing demand for sustainable energy solutions, particularly for energy supply in transient sensor systems, this study focused on environmentally friendly materials in organic photovoltaics (OPV) and their key photovoltaic parameters. The application of regenerated cellulose (RC), gelatin and propylene glycol (PGG) as biodegradable alternatives to fossil-based PET film substrates and soil-compatible carbon paste (SCP) as a replacement for evaporated metal electrodes was assessed for electronics. The investigated aspects included the current–voltage characteristics, leakage current, and cell efficiency under LED illumination at 1000 lx, relevant for IoT applications. Both the commercial and newly developed OPV components were then analyzed in terms of their microstructure, water solubility, and layer integration. Results showed that RC can serve as a promising alternative substrate for OPV, achieving a power conversion efficiency (PCE) of 15.88%, and the electrical properties of OPVs incorporating the developed SCP were significantly higher than those of the OPVs that used the commercial carbon paste (CP) electrode. SEM analysis confirmed good adhesion and uniformity between layers, supporting the mechanical integrity of the device. Despite the high leakage currents in devices with printed SCP electrodes, further optimization can improve the overall device performance. The water solubility and environmental impact of the OPV materials were assessed through conductivity and pH measurements over six months, revealing no significant changes in soil quality, with pH levels remaining within the plant-safe range of 6.0 to 7.5. The findings of this study demonstrate the performance of OPVs utilizing soil-compatible materials for transient electronics, towards fulfilling the requirements of energy autonomous sensing in digital agriculture applications while maintaining ecological integrity.

Received 27th June 2025
Accepted 3rd October 2025

DOI: 10.1039/d5ta05223h

rsc.li/materials-a

Introduction

Environmental challenges and the role of transient electronics in agriculture

Consideration of environmental aspects in electronics has become essential due to the increasing concerns on e-waste and the low availability of critical raw materials (CRMs).[1] Several global and European sustainability policies and actions, such as the EU's Green Deal and Circular Economy Action Plan and the United Nations Sustainable Development Goals (SDGs), are pushing researchers and industries to develop more sustainable products and services. Novel solutions of transient electronics, based on biodegradable or environmentally neutral components, are rapidly being developed and implemented in the field of ICT (information and communication technologies) for precision agriculture and agricultural IoT (Internet of Things) applications aimed at improving crop production and reducing food waste.[2]

Electronic devices and sensors for agricultural applications should be designed to avoid harmful ecological effects by utilizing soil-compatible and sustainable materials while meeting functional and performance requirements. Minimizing their overall impact requires a thorough assessment of both the materials and the manufacturing processes involved in producing each component. This includes reducing reliance on CRMs, minimizing the use of antibacterial silver, and adopting biopolymers as components that can be easily recycled or biodegraded. By focusing on sustainable materials and processes, these systems can provide vital agricultural insights while adhering to principles of ecological responsibility.[3–9] The work described herein targets applications such as the use of multisensory systems for the real-time monitoring of plant health and crop conditions through the continuous analysis of

[a]Łukasiewicz Research Network – Institute of Microelectronics and Photonics, St. Zabłocie 39, 30-701, Kraków, Poland. E-mail: beata.synkiewicz.musialska@imif.lukasiewicz.gov.pl

[b]VTT Technical Research Centre of Finland, P. O. Box 1100, Oulu, 90571, Finland. E-mail: marja.valimaki@vtt.fi

[c]VTT Technical Research Centre of Finland, P. O. Box 1000, Espoo, 02044, Finland

parameters such as soil or internal plant pH and temperature for the early detection of crop diseases, thereby enabling timely interventions and safeguarding agricultural productivity. A pivotal aspect of such a multisensory system is its power supply. To achieve environmentally sustainable energy harvesting through photovoltaics, research efforts are being directed toward the development of organic photovoltaic (OPV) devices.

Organic photovoltaics: opportunities and limitations

Organic photovoltaics are based on organic semiconductors, *i.e.*, carbon-based molecules or polymers, carrying out the photovoltaic effect *via* the absorption of sunlight or artificial light to produce electricity through charge transport.[10,11] In contrast, traditional photovoltaic (PV) panels rely on wafer-type crystalline silicon (c-Si) technology. However, silicon solar cells raise serious concerns regarding the accumulation of vast quantities of electronic waste at their end-of-life (EoL) stage. According to the International Renewable Energy Agency (IRENA), by 2030 and 2050, the total volume of discarded PV panels is expected to reach at least 2–8 million and 60–78 million tons, respectively.[12] Moreover, the extraction, refining and production processes of usable silicon are highly energy-intensive, and silicon was designated as a critical raw material by the European Commission in 2014.[13] As a result, many recent studies have focused on EoL management strategies for PV panels, particularly on recovery and recycling technologies for silicon. In this context, applications involving single-use and/or transient electronics can offer new possibilities for materials with tailored properties and alternative EoL scenarios.[14]

Materials for transient and biodegradable OPVs

Thin, lightweight OPVs with low environmental burden can be applied for energy harvesting in IoT-based systems designed for various applications, *e.g.*, sensing or tracking, as demonstrated by Sokka *et al.*[15] Therefore, while analyzing the biodegradability and applications of the various material options for use as OPV components in ICT, it is important to also consider the impact of those materials on their effectiveness for the intended purposes.

The base film, referred to as substrate, can comprise 40–80% of the weight of the thin-film device.[16] Polyethylene terephthalate (PET) is widely used in printed electronics due to its high optical transparency, good thermal stability and solvent resistance.[17] Although OPVs have been fabricated on paper,[18,19] most studies have focused on optically transparent cellulose nanofibers.[20,21] Studies exploring synthetic biopolymers have focused on naturally non-biodegradable materials, *e.g.*, poly(-lactic acid) (PLA).[16] Nonetheless, biodegradable materials, including those of natural origin, such as silk, gelatin, and natural resin shellac, have also been explored[22,23] and are of particular interest in the context of this study.

Metals and transparent conducting metal oxides are common materials used for hole and electron contacts, as well as for charge transport layers. Among them, indium tin oxide (ITO) is widely used[24] due to its high conductivity (8 to 12 Ω sq^{-1} sheet resistance on glass), optical transparency ($\sim$90%) and chemical stability.[25] At the same time, indium is a scarce resource, and its increasing demand raises concerns about its future availability. The use of alternative metal oxides, *e.g.*, ZnO, in energy-harvesting applications has been demonstrated at low light intensities.[26] Highly conductive oxide/metal/oxide structures, such as ZnO/Ag/ZnO or TiO_x/Ag/TiO_x, are also being developed as replacements for ITO, though they typically contain silver.[24,27] In addition, carbon nanotubes and graphene, conductive polymers, or composites combining metals with polymers are considered potential replacements for ITO.[24,28]

Poly(3,4-ethylenedioxythiophene) polystyrene sulfonate (PEDOT:PSS) is one of the most widely used transparent conducting polymers in organic photovoltaics. This is due to its compatibility with solution processing and its scalability through roll-to-roll (R2R) manufacturing using various wet-deposition techniques, such as printing and coating methods. It consists of a conjugated polymer, PEDOT, which carries a positive charge in its oxidized state, and a negative-charge-carrying polymer called PSS, which has deprotonated sulfonyl groups.

PEDOT:PSS is one of the most widely used electron-conducting organic polymers valued for its electrical conductivity, flexibility, optical transparency and water processability.[28,29] It does not exhibit any toxicity and can even be applied to living brain tissue.[30] However, its biodegradability remains incompletely understood and is still being investigated in the literature.[9,28,30] Notably, in one study, when PEDOT:PSS was combined with montmorillonite (MMT), an eco-biodegradability test showed that superworms consumed the hydrated composite at a rate of 0.046 mg h^{-1}.[9]

The selection of materials and manufacturing processes that can contribute to reducing the energy payback time is a key aspect of photovoltaic technology development. Therefore, efforts have been made to replace certain material components with more environmentally friendly materials sourced from renewable resources while utilizing low-energy-consuming production methods as replacements for processing under vacuum or inert atmosphere. An example of a low-energy-consuming process is screen-printing, and examples of studied materials are gelatin, carbon (graphite), and propylene glycol.[31]

This study aims to evaluate the potential of organic photovoltaic devices designed for transient electronics in digital agriculture for greenhouse use, utilizing environmentally benign, soil-compatible materials that support the sustainability of energy-autonomous sensor systems. Conventional OPV materials were replaced with biodegradable alternatives, such as gelatin mixed with propylene glycol, regenerated cellulose substrates, and carbon-based conductive pastes, to ensure ecological integrity. The impact of these materials on device performance and structural integration was thoroughly assessed using advanced microstructural analysis, water-solubility tests, and electrical and *JV* characteristic evaluations, providing a comprehensive understanding of their viability in sustainable OPV applications.

Materials and methods

The research was structured in three main phases: (i) selection and development of material components, (ii) characterization of materials and components, and (iii) fabrication and performance evaluation of organic photovoltaic devices.

During the material characterization phase, the properties of baseline reference materials were systematically assessed and compared with those of both commercially available alternatives and newly developed sustainable substrates and conductive layers. These evaluations included water-solubility tests, surface-roughness analysis, substrate–paste integration observation, electrical-conductivity measurements, and optical transmission (T) analysis. Based on the results, the optimal device configurations were selected, and test OPV structures with sustainable components were fabricated and subsequently evaluated in terms of their functional properties.

Selection and development of material components

Derived from collagen—the main structural protein in animal connective tissues—gelatin is a natural protein-based polymer. Its microbial degradation under natural environmental conditions typically occurs within weeks to months, depending on specific factors, such as temperature and humidity. Due to its lack of harmful chemicals and environmentally friendly properties, gelatin is increasingly utilized in sustainable packaging, with its application expanding into flexible substrates for microelectronics.

In this study, gelatin was selected as an alternative substrate for biodegradable OPV components, while propylene glycol (PG) was incorporated to enhance the film stability. Due to its widespread use in food, cosmetics, and pharmaceuticals, PG biodegradation is an important environmental consideration. Studies indicate that specific bacteria can efficiently degrade PG under controlled conditions, with optimal breakdown occurring aerobically in nutrient-enriched soil. Anaerobic degradation (50% less efficient than aerobic) also occurs, generating by-products, like propionic acid. However, complete mineralization is achieved with nitrate addition, preventing undesirable by-products.[32,33]

Due to its favorable properties and certifications for compostability in both industrial and home-composting environments, regenerated cellulose (NatureFlex™ 30 NVO, Futamura) with a thickness of 30 μm, later referred to as RC, was also selected as a biodegradable substrate, alongside the developed gelatin-PG films. To compare the functional performances of these biodegradable materials in OPV applications, a widely used fossil-based substrate: heat-stabilized polyethylene terephthalate (PET) film (Melinex® ST506, Mylar Specialty Films) with a 125 μm thickness, was included as a non-biodegradable industrial benchmark developed for printed electronics applications. This comparative framework enabled the evaluation of sustainable alternatives against established materials commonly employed in printed electronics.

Although silver was not directly classified as a Critical Raw Material in the EU's 2023 list, it is recognized as a strategically important resource, particularly in the context of renewable energy technologies. In contrast, the U.S. Geological Survey classifies silver as a CRM due to its essential role in technological, medical, and energy industries, highlighting its significance in applications, such as photovoltaics, electronics, and energy-storage systems. While the extraction of silver causes significant environmental repercussions (including pollution and high carbon footprint), choosing graphite as a conductive layer is environmentally and economically justified (99% graphite powder costing 10 EUR per kg makes it over 100 times cheaper than silver, *StoneX Bullion*, access: 18.02.2025).

The use of carbon powder in conductive pastes is becoming a common and environmentally friendly approach, as traditionally used conductive metals, such as silver, gold, and aluminium, are non-renewable resources with limited availability and costly recycling processes. In contrast, carbon can be sourced from renewable energy sources, such as biomass. Sustainable methods for graphite extraction include recycling of end-of-life batteries and industrial electrodes, which contribute to waste reduction and decrease reliance on CRMs. Furthermore, synthetic graphite can be synthesized from biomass sources, including lignocellulosic materials, such as wood and nutshells, through pyrolysis processes, promoting the utilization of renewable resources.[34,35]

PEDOT:PSS is considered an environmentally friendly conductive polymer because of its water-based form, biocompatibility, and high chemical stability, which may improve the lifespan of electronic devices. Its synthesis involves the polymerization of PEDOT using oxidizing agents, followed by complexation with PSS to form a stable aqueous dispersion. The production process is energy-efficient, utilizes low-toxicity reagents, and reduces environmental impact compared to conventional conductive materials. However, the biodegradability of PEDOT:PSS is yet to be fully explained in the literature.[28,30,36] Therefore, the application of commercial components containing both PEDOT:PSS and PEDOT:PSS as a binder for preparing a soil-compatible paste based on graphite is studied in this work.

Gelatin-PG-based film preparation

The films used as substrates (based on gelatin and propylene glycol, hereinafter referred to as PGG) were prepared using a modified tape casting method. A prepared amount of solid substance was dissolved in an aqueous solution at 60–90 °C until a homogeneous consistency was achieved. Subsequently, propylene glycol was added to the mixture, and the volume was adjusted to 500 mL with water. The resulting mixture was poured onto a silicone mold with a surface area of 0.24 m^2 and dried at room temperature with intensive air circulation for 24 hours. The manufacturing conditions (such as drying temperature and time, the ratio of solid components to solvent, and the amount of substance poured into the mold) were modified depending on the behaviour of the base material. A 40 μm thick PGG film was characterized and compared with PET and RC films.

Graphite-based paste preparation and printing conditions

Flake-shaped graphite powder (SINOGRAF, Poland) with a D_{50} of 5.0 μm, D_{90} of 10.0 μm, and carbon content greater than 96.1% was mixed with twice its mass of PEDOT:PSS (ELP 5015, Agfa-Gevaert, Belgium) and ground in agate mortar for about 20 min. The developed soil-compatible carbon paste (SCP) based on graphite and PEDOT:PSS was screen-printed (printer ZUT, Poland) using a screen with a mesh size of 150 and a squeegee set at a 45° angle. After printing the layers on the substrate, they were cured for 15 min at 80 °C. The temperature in the laboratory during the screen-printing process was 22 °C. For comparison, a commercial carbon paste (CP) (EDAG 407A, Loctite, USA) was used as a reference, and screen-printed layers based on it were developed and tested under the same conditions as those used for the SCP.

Characterization of materials and components

The optical transmission of substrate materials was measured with a UV-Vis-NIR spectrophotometer (Cary 5000, Agilent).

The surface roughness was measured with a white light interferometer (WLI Contour X-500, Bruker) with 10× magnification and plane fit (tilt). The arithmetic roughness (S_a) was calculated by fitting the absolute surface profile data with the mean surface level, root-mean-squared roughness (S_q) by fitting the root-mean-squared data from the surface profile with the mean surface level, and maximum height (S_z) by defining the sum of the largest peak height value and the largest pit depth value within the definition area.

The sheet resistance of the conductive layers (printed with soil-compatible paste – SCP) was measured in ohms/square, as the resistance between the two electrical contacts using a multimeter (Keithley Instruments, USA).

Tensile strength tests were conducted on an industrial tensile testing machine using input samples with dimensions of 15 × 60 mm. Due to the varying thicknesses of the foils, the cross-sectional areas of the samples differed accordingly. The test involved two sets of trials: one set was performed on samples before exposure to a thermal shock chamber and the other set after exposure. Each set consisted of two measurements. The objective of the test was to observe the total elongation of the samples under the application of longitudinal force. During the test, the samples were symmetrically clamped in a jaw holder with a width of 15 mm. The test was carried out until the complete rupture of the samples occurred. The applied force was measured in Newtons, while the elongation was recorded as a percentage in 24 cycles of +120/30 min and −55/30 min.

The morphology and microstructure of OPV components in various configurations were characterized using the Quattro ESEM microscope (Thermo Fisher Scientific) equipped with FEG (field emission gun, ETD, Everhart-Thornley detector). SEM images of the sample cross-sections and surfaces were obtained in LVD (low vacuum detector) mode at magnifications of 100–20 000×, with an accelerating voltage of 3–15 kV.

To evaluate the stability and degradation behavior of the materials intended for use in OPV devices under aqueous conditions, the water solubility of the selected components was examined by measuring the conductivity and pH value of water containing the samples.

The laboratory test station was prepared, focusing on the sterilization of containers to prevent any potential contamination. Samples were then prepared by mixing 1 g of each material with 100 mL of water, ensuring three replicates for each type to guarantee statistical reliability. The initial weights of the samples were accurately recorded before they were fully immersed in the water-filled containers. The initial pH levels and conductivity of the water were measured to provide a baseline for future comparisons. During the incubation phase, containers were placed in a controlled temperature environment, with temperatures set between 20 °C and 23 °C, and the system was sealed to maintain consistency. The incubation periods varied, ranging from 1 to 24 hours and extending up to one week, to capture a broad spectrum of material behaviour over time. At predetermined intervals within these periods, the samples were carefully removed, dried, weighed, and their weights recorded alongside the specific dates and times of sampling. Additionally, the pH of the water solution after sample removal and the conductivity of the solution were measured to determine the potential influence of the dissolved samples on the soil.

For determining the strength of the layers printed using CP and SCP, bending tests were carried out for the conductive layers screen-printed on the PET substrate. For this purpose, a dedicated bending tool with a bending diameter of 1 cm (bending radius of 5 mm) was fabricated using 3D printing technology with a BambuLab AMS X-1 Carbon printer, employing transparent PETG material (PETG trans EXTRUDR brand). Prior to the bending tests, the sheet resistance of each printed layer was measured using a Brymen brand BM 857S multimeter. For each type of paste (CP and SCP), 6 sheet-resistance measurements were taken. Subsequently, bending tests were conducted using the previously printed devices. Each sample underwent 1000 bending cycles (180°, u-shape bend). After this procedure, the sheet resistance of the printed layer was measured again following the same methodology. The relative change in resistance was determined according to the following equation:

$$\Delta R\,[\%] = ((R_2 - R_1)/R_1) \times 100$$

R_1 – initial sheet resistance before bending, R_2 – sheet resistance after bending.

Average values were calculated for each sample after bending and compared with previous measurements (as mentioned in IEC 62899-202-5:2018 standard).

Fabrication and performance evaluation of organic photovoltaic devices

The standard device configuration with an active cell area of 33 mm^2 was fabricated by preparing PET/H30/PEDOT:PSS/NF3000/LiF/Al and RC/H30/PEDOT:PSS||NF3000/LiF/Al structures. Biopolymer-based hybrid (H30) coating (H30 BrightBio, BrightPlus) was deposited on PET and RC substrates using slot-

die coating (RLC coater, Infinity PV). PEDOT:PSS ink, for the hole-contact layer, was prepared by mixing PEDOT:PSS (Clevios PH1000, Heraeus), isopropyl alcohol and ethylene glycol in a ratio of 73 : 22 : 5 by weight. A triple layer of PEDOT:PSS was gravure-printed on H30-coated PET and RC substrates (Labratester, Norbert Schläfli Maschinen). The PEDOT:PSS layer, with a 30 nm thickness, was gravure-printed with ink prepared by mixing PEDOT:PSS (Clevios Al4083, Heraus Germany) and IPA in a ratio of 77 : 23 by weight. NF3000-P and NF3000-N, combined in a ratio of 1 : 1 by weight and used in the active material ink, were dissolved in *o*-xylene : 1,8-diiodooctane (DIO) in 99.5 : 0.5 by volume. Active layers, *i.e.*, layers with a 152 nm-layer thickness, were prepared by spin coating (WS-650Mz-23NPPB, Laurell) on PEDOT:PSS. All wet deposited layers were dried at 80 °C. Devices were finalized with 1.5 nm LiF and 100 nm aluminium thermally evaporated top electrodes.

The inverted device configuration with an active cell area of 15 mm^2 was fabricated by preparing PET/ITO/ZnO/poly(3-hexylthiophene):[6,6]-phenyl C61 butyric acid methyl ester (P3HT:PCBM)/PEDOT:PSS/Carbon. Layers below the top electrode were processed as reported in the paper by Välimäki *et al.*[16] Top electrode (hole contact) comprised either screen-printed SCP or CP, or evaporated 1 nm of MoO_3 and 100 nm of Ag, with the active cell area of 25 mm^2. Schematic diagrams of the standard and inverted device configurations, together with the cell layout, are presented in Fig. 1. The sheet resistance of single-cell OPV devices was measured using a four-point probe setup with a voltage source meter (Keithley 2400). IV measurements were executed using an LED light source (colour temperature: 4100 K) comparable to the lamps used in growth chambers and the voltage source meter (Keithley 2400). The illuminance value of 1000 lx and the light source spectrum were measured using an illuminance Spectrophotometer (CL-500A, Konica Minolta), and the light intensity (0.3045 mW cm^{-2}) was calculated by integrating the individual spectrum.

Results and discussion

Substrates and device structures on the biodegradable substrate

The substrates and printed thin-film layers on top of the biodegradable substrate were characterized prior to the fabrication of single-cell OPV devices. The RC substrate was surface-coated to enable the wet deposition of a thin-film device. The standard device architecture was fabricated on top of the RC substrate, and in the inverted device architecture, the metal top electrode was replaced with SCP. Table 1 presents the S_a, S_q, and S_z of the studied substrates and thin-film layers for the fabricated OPVs.

S_a describes the height difference of each point with respect to the arithmetical mean of the surface, and S_q describes the standard deviation of the heights. PET has been developed for flexible electronics, providing good thermal, mechanical, optical and surface properties, including low surface roughness. The RC substrate resulted in S_a and S_q values that were an order of magnitude higher (98 nm and 158 nm) than those for PGG (70 nm and 128 nm, respectively). In the standard device structure, S_q and S_q were increased to 179 nm and 246 nm after PEDOT:PSS printing and to 179 nm and 246 nm after NF3000 printing.

Fig. 2 presents the surface profiles of the PET, RC and PGG substrates, and those of coated H30, printed PH1000, NF3000, CP and SCP for OPVs. The surface roughness values of the layers prepared on RC were primarily dependent on the underlying surfaces, as shown in Fig. 2. Thus, high S_a, S_q, and S_z values describing the sum of the largest peak heights hold a significant impact on the wetting and quality of the printed layers.

The baseline PET substrate surface profile is uniform and does not contain high peaks or large defects, while the RC surface consists of several peaks and the PGG surface has a few. The cross-section profile shows that the height of these peaks ranges from a few hundred nanometres to micrometres. H30 coating can cover smaller peaks, but hardly the peaks that are several micrometers high. Gravure-printed PH1000 and NF3000 layers appear visually uniform; however, the surface profile shows that the ink partially copies the engraved pattern of the printing plate, while the variations of the CP and SCP surfaces can be correlated to the size of carbon particles. The CP paste, being less viscous, spreads evenly during screen printing and does not hold the screen pattern as clearly as the SCP paste. These adjustments ensure consistent print quality. In the case of PEDOT:PSS, the surface profile of the substrate may significantly influence the uniformity and electrical conductivity of screen-printed layers, with smoother surfaces supporting more consistent film properties.[9]

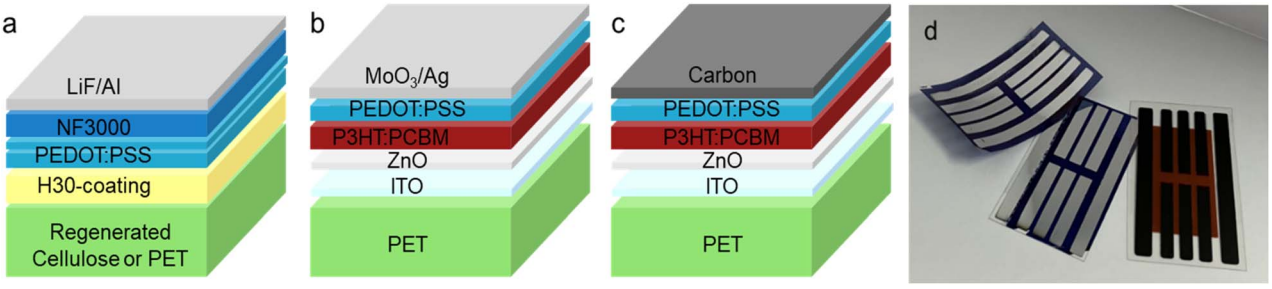

Fig. 1 Illustration of (a) the standard and (b and c) the inverted device structure. (d) Photograph presenting the layouts, each comprising six single-cell OPVs.

Table 1 Mean arithmetic roughness (S_a), root-mean-squared roughness (S_q), and total roughness height (S_z) of substrates and OPV layers on top

Sample	S_a [nm]	S_q [nm]	S_z [μm]
PET	9 ± 4	14 ± 7	1 ± 1
Regenerated cellulose film (RC)	98 ± 30	158 ± 32	4 ± 1
Propylene glycol–gelatin film (PGG)	70 ± 20	128 ± 76	5 ± 2
RC/H30	119 ± 29	181 ± 48	3 ± 1
RC/H30/PEDOT:PSS	166 ± 19	235 ± 25	4 ± 1
RC/H30/PEDOT:PSS/NF3000	179 ± 64	246 ± 74	4 ± 0
PET/ITO/ZnO/P3HT:PCBM/PEDOT:PSS/CP	996 ± 95	1416 ± 240	15 ± 5
PET/ITO/ZnO/P3HT:PCBM/PEDOT:PSS/SCP	12 866 ± 2428	15 111 ± 2504	62 ± 9

Due to the fact that the commercial CP paste has lower viscosity than the SCP paste (influenced, among other factors, by the degree of grain refinement), during the screen-printing process, it spreads more evenly across the printed surface and does not retain the screen mesh pattern (the characteristic square matrix) on its surface as prominently as the SCP paste does. The mesh parameters in screen printing, such as screen tension and mesh count, directly affect the resolution and thickness uniformity of the printed layers.

It should be emphasized that the irregularities of the surface caused by the mesh pattern represent only a small part of the total print height. Drying conditions play a crucial role in determining the mechanical and electrical stability of PEDOT:PSS films as rapid drying can introduce internal

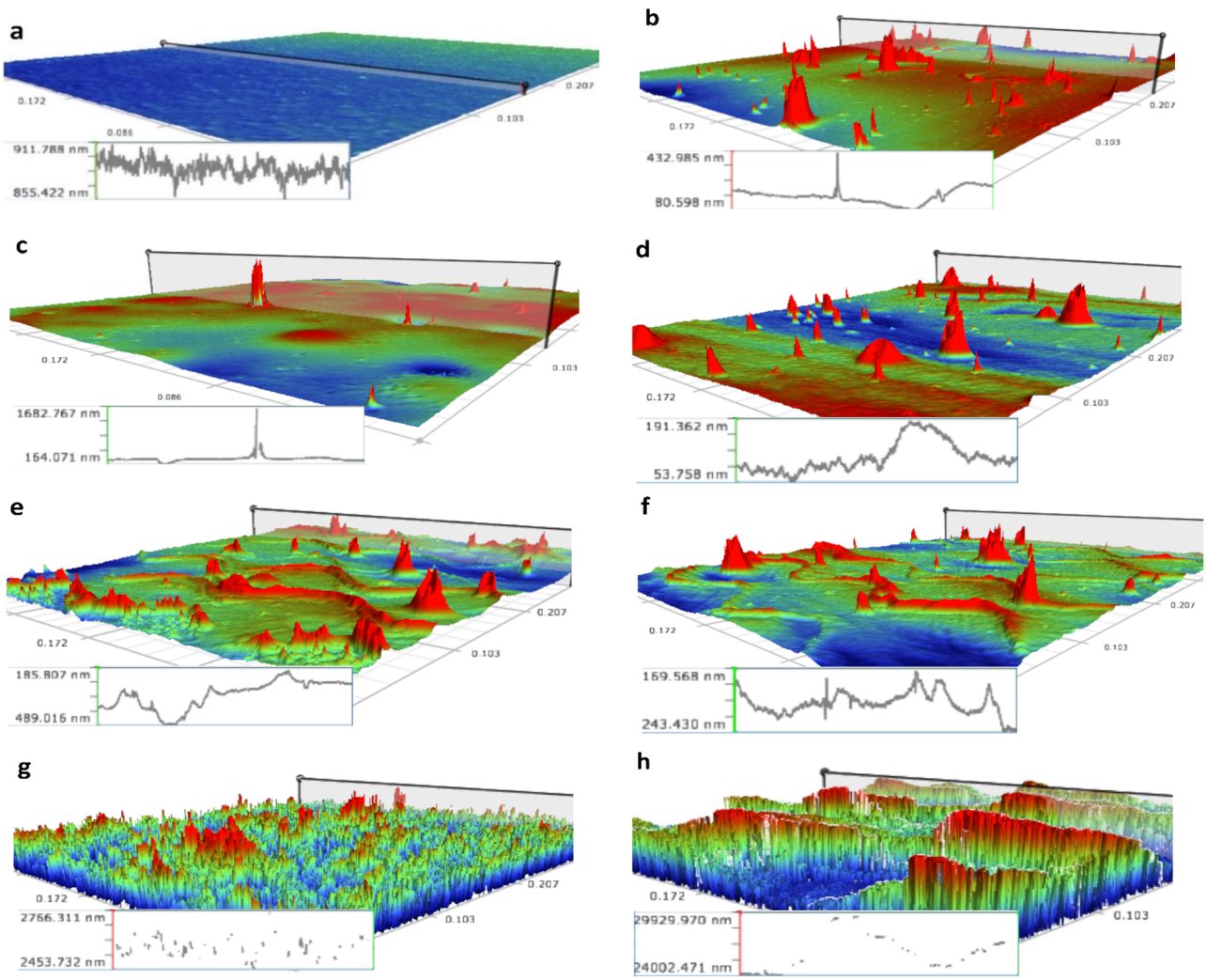

Fig. 2 Surface profiles of (a) PET, (b) RC, (c) PGG, (d) H30, (e) PH1000, (f) N3000, (g) CP and (f) SCP. Materials (d and e) deposited layer-by-layer on RC and layers (g and h) on PET/ITO/ZnO/P3HT:PCBM/PEDOT:PSS.

stresses, leading to microcracks and reduced reliability.[9] In this case, the surface irregularities caused by the mesh pattern did not significantly affect the resistance of the conductive layer in the studied samples.

Fig. 3 presents the optical transmission of the studied substrates. In comparison to that of PET, the optical transmissions of RC and PGG were slightly higher in the visible-light region, being 89–92% and 90–92%, and comprising wider regions at lower wavelengths than that for the reference PET, as shown in Fig. 3. The transmission of RC was 27% and PGG 76% at 300 nm, while for PET, the value dropped to zero. The transmission of the H30-coated RC was comparable to the transmission of RC. A high optical transmission is beneficial if the application, *e.g.*, sensing, needs to operate in the UV-A or UV-B region.

Single-cell OPV performance evaluation

In earlier studies, gravure-printed PEDOT:PSS on the PET substrate resulted in uniform printing quality and sheet resistances of 244 Ω sq^{-1} (90 nm) and 461 Ω sq^{-1} (50 nm).[16] In this work, the thickness of PEDOT:PSS was increased to compensate for the higher surface roughness of the RC substrate and to reduce the sheet resistance to ≤150–200 Ω sq^{-1} by printing single, double and triple layer structures. During the printing process, the PGG substrate showed insufficient thermal stability, causing non-planarity of the substrate. For that reason, gravure printing of PEDOT:PSS was executed only on the PET and RC substrates. The sheet resistances of the gravure-printed PEDOT:PSS for the hole contact on top of PET, H30-coated PET and H30-coated RC are depicted in Table 2.

The increase in the thickness of PEDOT:PSS from a double to a triple layer resulted in a significant decrease in the sheet resistance, being slightly lower on PET and significantly lower on the H30-coated PET and RC. As a result, the gravure-printed PEDOT:PSS on the H30-coated RC reached the targeted sheet resistances of 175 Ω sq^{-1} (double layer) and 113 Ω sq^{-1} (triple layer). Thus, the lowest sheet resistance of the printed PEDOT:PSS was reached on the RC.

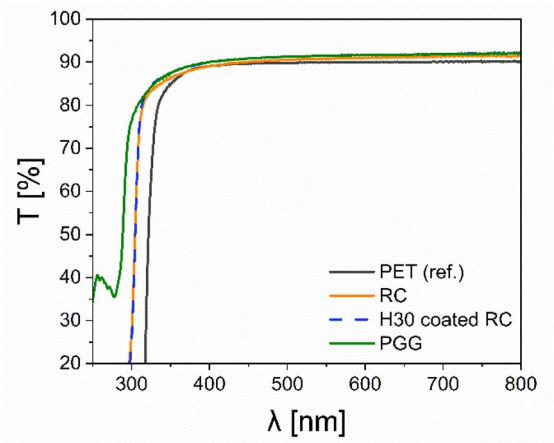

Fig. 3 Optical transmission (*T*) of the PET, RC, H30-coated RC and PGG substrate.

OPV cells with a standard device configuration were fabricated on the RC and PET films to study the replacement of fossil-based substrates with soil-compatible ones. IV measurements were executed under 1000 lx lighting conditions, comparable to the conditions in typical indoor-OPV related studies and under shaded leaves in greenhouses.

Fig. 4a shows that the lower V_{oc}, together with the high leakage current in the averaged *JV* characteristics, leads to a slight decrease in all electrical properties. However, the shape of the *JV* curve of the maximum power conversion efficiency (PCE) cells is comparable to that for the cells on PET. Cells fabricated on RC reached a PCE of 15.88%, while cells on PET had a maximum PCE of 23.29% (Table 3).

The obtained results point out the potential of RC film as an OPV substrate, despite the challenges caused by the high surface roughness.

High surface roughness and peaks challenge the uniformity of printed layers, which would most likely impact the device performance. In addition, limitations in thermal processing and handling of the 30 μm-thick substrate, in comparison to the reference-PET, impact the quality of the printed device structure.

In a study by Sokka *et al.*, eight serially connected cells with a total size of a credit card were able to provide 2.19 V and 64 μA at maximum power point in an LED light at 1000 lx, guaranteeing the energy required for the NFC-based temperature monitoring and data-logging system.[15] In this work, the electrical properties of NF3000-based cells enable them to provide sufficient energy for a similar sensing system even with using regenerated cellulose as a substrate, as the V_{oc} and J_{sc} values reached 0.66 V and 140 μA cm^{-2}, respectively. To study the replacement of the evaporated metal top electrode with printed carbon, OPV cells with an inverted structure were used. The devices were fabricated using the well-established ITO-PET substrate to minimize variables.

Averaged *JV*-curves for both carbon top electrodes in Fig. 4b, showing high leakage current and low fill factor, which result in a significant reduction in performance. Although a high variation between the produced cells was observed, the maximum PCE cells with printed carbon showed significantly lower leakage current and increased fill factor.

Cells with SCP reached a PCE of 1.98%, with V_{oc} of 0.42 V and J_{SC} of 51 μA cm^{-2} (Table 3). Compared to the commercial carbon paste used, with a V_{oc} of 0.31 V and a J_{sc} of 27 μA cm^{-2}, the soil-compatible paste fabricated in this work is more compatible with the fabricated OPV layers. The cell structure used was not optimized for the low light intensities, as evidenced by the low performance of the reference cells with the evaporated silver top electrode. The obtained results show that the printed SCP can be a potential alternative for fully printed soil-compatible OPVs, but its performance improvement requires the optimization of the device structure.

Further studies on the feasibility of transient OPVs for agricultural applications need to explore biodegradable encapsulation and stability testing.

Table 2 Sheet resistance of the gravure-printed PEDOT:PSS (PH1000) on PET, H30-coated PET and H30-coated regenerated cellulose substrate

PH1000	R [Ω sq^{-1}] on PET	R [Ω sq^{-1}] on H30/PET	R [Ω sq^{-1}] on H30/RC
Single layer	328 ± 12.4	15.2 k ± 3.56 k	462 ± 19.5
Double layer	142 ± 15.7	1.12 k ± 0.21 k	175 ± 7.26
Triple layer	130 ± 12.5	163 ± 11.7	113 ± 6.81

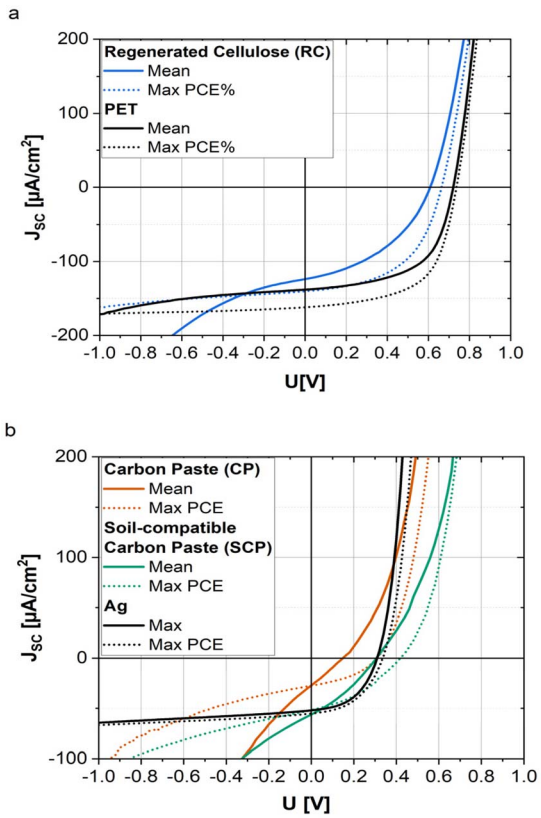

Fig. 4 J–V characteristics of the fabricated device structures under LED @ 1000 lx of (a) using RC and PET substrates, and (b) CP, SCP and Ag top electrodes.

Microstructural and compositional observations of the device/layers

The SEM images of the commercial carbon paste (CP) and the in-house carbon paste (SCP) are shown in Fig. 5–7. The CP layer is more homogeneous, whereas the SCP layer contains more pores and visible particle boundaries and is generally less uniform. This difference in the microstructure may be due to the difference in the preparation methods used by the manufacturers of the commercial paste. Generally, images in high magnification show no significant inhomogeneity (irregularities, interfacial defects) of the SCP layer, and the adhesion of the printed layer to the substrate is confirmed. No relevant delamination or the presence of an interlayer resulting from the reaction with the substrate was observed at the SCP layer–substrate interface (Fig. 7a and b). However, increased porosity can be observed in the SCP layer, compared to the case for the CP layer, revealed at higher magnification in the cross-sectional view, which may indicate a potential source of current leakage. In such regions, the electrical current does not flow uniformly but is concentrated in narrow pathways (so-called current crowding), which can lead to increased resistance, local overheating, and the formation of micro-breakdowns (leakage currents). Moreover, the increased porosity may affect the contact resistance between the conductive layer and the substrate. A reduced effective contact area caused by pores leads to increased local contact resistance, which in turn enhances the non-uniform distribution of current and further promotes current crowding effects.

Fig. 6 shows SEM images of the cross-section, and Fig. 7 shows the top view of SCP and CP on the RC and PET substrates. Both pastes exhibit better adhesion to the RC substrate in comparison to the PET substrate. This could be due to the organic nature of the RC (regenerated cellulose) film, which binds better to the organic carbon paste screen-printed on it.[37]

Bending tests of the printed conductive layers

In the provided study, the SCP material exhibited an increase in sheet resistance in the range of 20.7% after 1000 bending cycles (180° bending, 5 mm radius), while the CP material showed

Table 3 Mean, [std] and (max) electrical properties of the fabricated device structures under LED @ 1000 lx

Stack	V_{oc} [V]	J_{sc} [μA cm^{-2}]	FF	PCE [%] [std.]
Substrate: replacement of PET with regenerated cellulose (RC)				
PET/H30/PEDOT:PSS/NF3000/LiF/Al	0.72 (0.74)	138 (162)	0.58 (0.59)	18.83 [2.24] (23.29)
RC/H30/PEDOT:PSS/NF3000/LiF/Al	0.60 (0.66)	124 (140)	0.46 (0.52)	11.10 [2.23] (15.88)
Hole contact: replacement of Ag with carbon paste (CP) and soil-compatible carbon paste (SCP)				
PET/ITO/ZnO/P3HT:PCBM/MoO_3/Ag	0.31 (0.34)	52 (55)	0.48 (0.46)	2.55 [0.18] (2.82)
PET/ITO/ZnO/P3HT:PCBM/PEDOT:PSS/CP	0.18 (0.31)	27 (27)	0.31 (0.39)	0.54 [0.39] (1.09)
PET/ITO/ZnO/P3HT:PCBM/PEDOT:PSS/SCP	0.34 (0.42)	56 (51)	0.32 (0.37)	1.98 [0.50] (2.61)

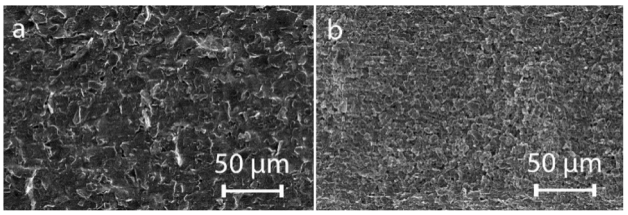

Fig. 5 Surface SEM images of screen-printed layers of (a) carbon paste and (b) soil-compatible carbon paste.

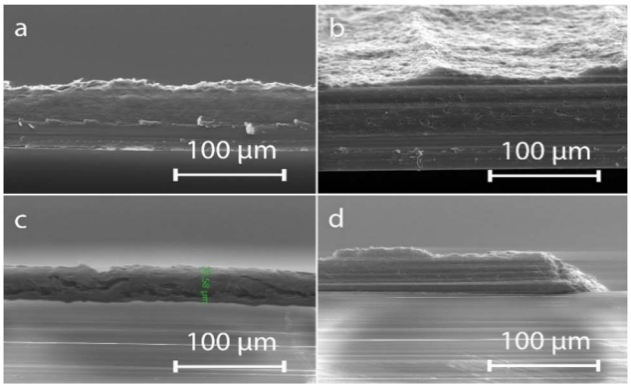

Fig. 6 Cross-sectional SEM images of the screen-printed layers of (a) carbon paste on RC, (b) soil-compatible carbon paste on RC, (c) carbon paste on PET and (d) soil-compatible carbon paste PET.

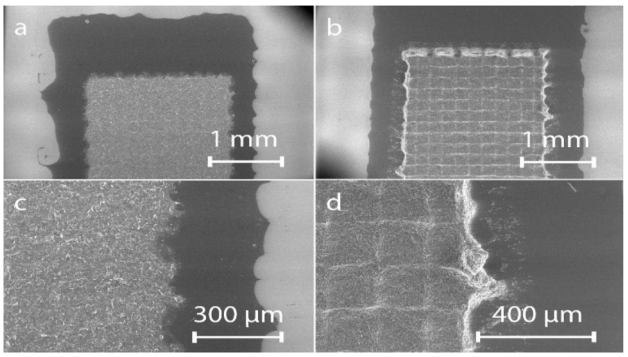

Fig. 7 Surface SEM images of PET/ITO/ZnO/P3HT:PCBM/PEDOT:PSS/carbon paste (a and c) and PET/ITO/ZnO/P3HT:PCBM/PEDOT:PSS/soil carbon paste (b and d).

a slightly broader variation in resistance depending on the sample, reaching 21.1%. For the SCP paste on PET, the sheet resistance increased from an average value of 42.3 Ω sq^{-1} to 51.1 Ω sq^{-1} after the bending tests. For the CP paste, it increased from an average value of 35.67 Ω sq^{-1} to 43.3 Ω sq^{-1}.

These values fall within the generally accepted range (for printed conductive layers subjected to cyclic mechanical stress, increases of up to 30% after 1000 cycles at a 5 mm bending radius are considered tolerable). It should also be emphasized that the investigated samples are not intended for applications involving continuous dynamic bending, but rather for use in flexible or unconventional substrates exposed only to occasional mechanical deformation. Under such conditions, the observed changes in resistance can be regarded as acceptable and indicative of sufficient mechanical durability.

Water solubility of the device/components

Gelatin, with a low water content (protein polymer), exhibits the characteristics of a typical rigid substance with minimal plasticity.[38] This moisture dependence explains the mechanical variability of gelatin-based films under different environmental conditions.

Propylene glycol (PG), a hygroscopic diol, interacts physically and chemically with gelatin, enhancing its water retention and modifying its hydration behaviour. This results in gelatin films with coexisting flexible and brittle regions, depending on moisture content and drying process. Such sensitivity to humidity leads to dimensional changes, phase separation, and surface irregularities—factors that critically affect the stability and function of biodegradable electronic devices.

Maintaining controlled humidity and temperature during layer deposition minimizes these effects, resulting in uniformity and defect reduction. In this context, gelatin's responsiveness to moisture becomes not only a challenge but also an asset because it enables rapid biodegradability, making gelatin-based materials ideal for transient electronic systems. Additionally, as reported in the literature, gelatin films demonstrate complete degradation within 24 hours in aqueous environments, in contrast to synthetic polymers, such as PLA (38.0% ± 4.3%) and PVA (56.3% ± 0.7%), which degrade much more slowly under the same conditions.[39,40]

Despite the numerous advantageous properties of gelatin-based substrates, components deposited on regenerated cellulose were selected for water solubility tests, taking into account the need to balance the degradation time of OPV device components in aqueous environments.

Over a period of six months, OPV samples containing regenerated cellulose (RC) film, RC with H30 coating, RC with H30 coating and PEDOT:PSS, and RC with H30 coating plus an aluminum (Al) top electrode exhibited a mass increase ranging from 170.52% to 212.85%. These results, based on water-immersion tests, indicate the substantial water absorption of the samples and their pronounced tendency to disintegrate in aqueous environments. The high water uptake is likely to enhance the migration of microorganisms into the material structure, thereby promoting biodegradation processes.

The electrical conductivity is an important parameter in soil quality control because within the range of 600 μS cm^{-1} to 5000 μS cm^{-1}, it significantly influences chemical processes such as ammonia volatilization and microbial processes (*e.g.* ammonification, nitrification, denitrification, decomposition of organics and respiration).[41] Changes in the conductivity of the water containing materials selected for OPV after 6 months of immersion are presented in Fig. 8a. The initial conductivity of water samples was 60 μS cm^{-1}. Like the increase in pH, water containing the RC substrate exhibited the highest increase in conductivity (up to over 70 μS cm^{-1}). The most significant

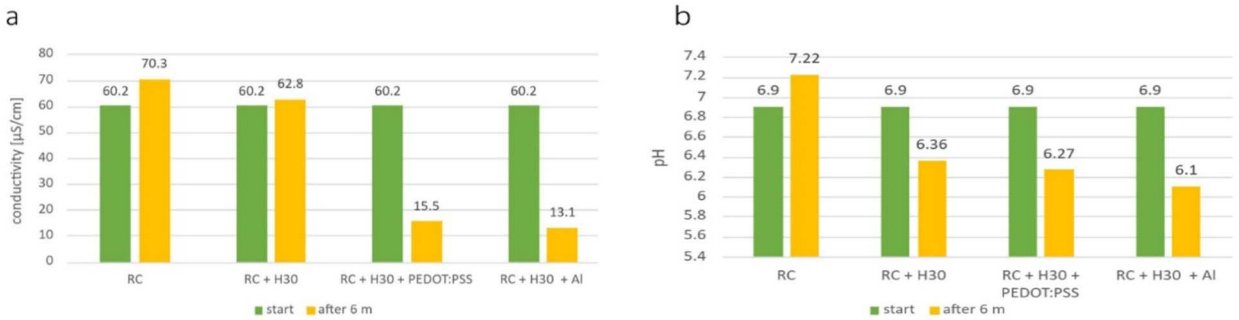

Fig. 8 Changes in (a) conductivity (μS cm^{-1}) and (b) pH of water containing OPV samples with regenerated cellulose (RC) film, RC + H30 coating, RC + H30 coating + PEDOT:PSS and RC + H30 coating (H30) + Al top electrode after 6 months.

change in conductivity was observed for the multi-layered samples containing the RC substrate, H30-coating and aluminium top electrode. The conductivity in this case decreased by 50 μS cm^{-1}. Uncoated RC tends to increase the conductivity of the water, whereas an additional layer of H30 coating reduces the effect of leaching into the water. On the other hand, added layers of PEDOT:PSS and Al were found to decrease the conductivity of water over time, probably due to ion adsorption or barrier mechanisms. However, none of these changes are significant enough to shift the electrical conductivity of the soil to unsafe limits unless it is already very polluted. Therefore, overall, the influence of all the materials in the study on soil conductivity is negligible and the proposed device does not pose any threat to the soil health, plants and microorganisms.

The measure of the hydrogen-ion (H^+) activity in the soil solution is called soil acidity or pH. The pH of the soil mainly influences the toxicity and bioavailability of elements, such as Fe, Mn, B, Cu, Cd, Al and others, to plants and microorganisms.[41,42] Usually, there is no significant effect on the plant roots and microorganisms in the soil within the pH range of 6 to 7.5, and the majority of the nutrients are readily available within this range.[41] Over a period of 6 months, the pH of the water decreased for all the samples with RC coating by an average of 0.68 pH units, as shown in Fig. 8b. However, in the case of the uncoated RC substrate, the pH of the water increased by 0.32 units. The changes in the pH of the water samples containing the various components of the developed OPV device in this study remained within this pH range, which is safe for plants. Both the increase in pH for water samples with uncoated RC and the decrease in pH for water samples containing coated RC were not significant enough to disturb the processes of nutrient uptake in the soil. Moreover, the study was conducted in closed containers where the water could not be dispersed. However, during agricultural applications, the water in the soil will be more dispersed and the changes in pH of the water surrounding the OPV are expected to be less pronounced than the changes observed in this study. This indicates that the materials used in this study are safe for applications in agriculture and may remain in the soil without causing any negative impact on the crops and the surrounding environment.

Conclusions

Agriculture faces enormous challenges in fulfilling the needs of the growing population without exhausting natural resources, *i.e.*, how to grow more using fewer resources while minimizing losses and environmental impact. One of the key considerations is how to enhance operational efficiency and prevent crop losses under rapidly changing growing conditions. New plant diseases and unprecedented weather conditions caused by climate change are reasons for the growth of precision and digital agriculture, relying on the use of sensing and monitoring devices to tackle these challenges. In precision agriculture, sensing technologies are used for gathering data on the crop and plant conditions to increase farm productivity through the early detection of plant diseases and harmful conditions.[2] The work presented in this article confirms the possibility of using biodegradable and soil-compatible materials in organic photovoltaics as transient electronic devices, achieving both environmental benefits and functional performance.

The replacement of fossil-based PET with regenerated cellulose (RC) resulted in NF3000-based standard-configuration OPV cells with an advantageous power conversion efficiency (PCE) of 15.88%. The excellent PCE and high optical transmission in the visible range (89–92%) validate RC as a competitive, compostable substrate. While the propylene glycol–gelatin (PGG) films showed promise, processing challenges due to thermal sensitivity and water absorption highlighted the need for further material optimization, including potential cross-linking or wax modification.

The developed soil-compatible carbon paste (SCP) performed significantly better as an electrode than the commercial alternative in P3HT:PCBM-based inverted-configuration OPV cells, resulting in a PCE of 1.98%, with V_{oc} of 0.42 V and J_{sc} of 51 μA cm^{-2}. The obtained values are relatively close to those of the reference cells with a metal-based top electrode. The efficiency of the fully printed inverted OPV can be increased by using a high-performing donor–acceptor blend. The ecological advantages and compostability of the fabricated OPVs provide opportunities for employing fully degradable devices in applications where high performance is important but not the primary requirement.

This design approach can contribute to transforming agricultural models (where advanced sensing systems are essential) into more environmentally sustainable models by preventing the release of unnecessary and harmful chemical substances into the environment. However, its implications extend beyond agriculture. The proposed materials and device structures are also suited for health monitoring and other sectors relying on single-use electronics, where environmental exposure or high-volume disposal is a concern. Compostable or safely decomposing OPV components can significantly reduce the risk of microplastic release and contribute to the circular economy.

Future research will focus on improving the long-term stability of biodegradable layers, scaling up fully printed devices, and assessing degradation behaviour in real soil environments.

Author contributions

Beata Synkiewicz-Musialska: conceptualization, methodology, formal analysis, data curation, writing – original draft, writing – review & editing, supervision. Marja Välimäki: conceptualization, methodology, formal analysis, investigation, visualization, writing – original draft, writing – review & editing, supervision. Kaisa-Leena Väisänen: methodology, investigation, data curation, formal analysis, visualization, writing – original draft, writing – review & editing. Kiranmai Uppuluri: methodology, investigation, data curation, formal analysis, writing – original draft, writing – review & editing. Krzysztof Szostak: data curation, formal analysis, visualization. Maria Smolander: conceptualization, writing, reviewing and editing, supervision, project administration, funding acquisition. Liisa Hakola: conceptualization, writing, reviewing and editing, project administration, funding acquisition.

Conflicts of interest

There are no conflicts to declare.

Data availability

The data that support the findings of this study are available on Zenodo at **https://zenodo.org/records/17087378**.

Acknowledgements

The authors want to acknowledge Anne Peltoniemi, Jenni Tomperi and Minna Kehusmaa for their excellent technical assistance. This research was supported by the CHIST-ERA project Transient Electronics for Sustainable ICT in DigitaL Agriculture (Research Council of Finland Grant No. 350411) and the National Science Centre, Poland, under CHIST-ERA IV Programme, under Grant Agreement no 857925. Further support was provided by the Research Council of Finland Flagship Programme, Photonics Research and Innovation (PREIN), decision number 346545. Part of the facilities used were provided by the Research Council of Finland Research Infrastructure Printed Intelligence Infrastructure PII-FIRI, Grant No. 358621.

Notes and references

1 J. M. van Gaalen and J. C. Slootweg, *ChemSusChem*, 2024, **18**, e202401170.
2 R. P. Sishodia, R. L. Ray and S. K. Singh, *Remote Sens.*, 2020, **12**, 1–31.
3 C. Yang, W. Lin, Z. Li, R. Zhang, H. Wen, B. Gao, G. Chen, P. Gao, M. M. F. Yuen and C. P. Wong, *Adv. Funct. Mater.*, 2011, **21**, 4582–4588.
4 K. Dušek, D. Koc, P. Veselý, D. Froš and A. Géczy, *Adv. Sustainable Syst.*, 2024, 2400518.
5 B. Synkiewicz-Musialska, M. Välimäki, K. L. Väisänen, R. Cichocki, K. Uppuluri and B. Sikora, *SciRad*, 2024, **3**, 212–217.
6 T. Punkari, A. Kattainen, A. Fonseca, J. Pronto, J. Keskinen and M. Mäntysalo, *IEEE J. Flex. Electron.*, 2024, **4**, 12–19.
7 C. Mevada, J. Tissari, V. S. Parihar, A. Tewari, J. Keskinen, M. Kellomäki and M. Mäntysalo, *J. Mater. Chem. A*, 2024, **12**, 24357–24369.
8 K. Uppuluri, D. Szwagierczak, L. Fernandes, K. Zaraska, I. Lange, B. Synkieiwcz-Musialska and L. Manjakkal, *J. Mater. Chem. C*, 2023, **11**, 15512–15520.
9 E. Luoma, M. Välimäki and K. Immonen, *J. Appl. Polym. Sci.*, 2023, **140**, 1–13.
10 M. Ylikunnari, M. Välimäki, K. L. Väisänen, T. M. Kraft, R. Sliz, G. Corso, R. Po, R. Barbieri, C. Carbonera, G. Gorni and M. Vilkman, *Flex. Print. Electron.*, 2020, **5**, 1–n.
11 T. Ameri, G. Dennler, C. Lungenschmied and C. J. Brabec, *Energy Environ. Sci.*, 2009, **2**, 347–363.
12 S. Weckend, A. Wade and G. Heath, *End-Of-Life Management: Solar Photovoltaic Panels*, International Renewable Energy Agency (IRENA), 2016.
13 A. Jäger-Waldau, *PV Status Report*, European Commission, 2014.
14 A. K. Jaiswal, V. Kumar, E. Jansson, O. H. Huttunen, A. Yamamoto, M. Vikman, A. Khakalo, J. Hiltunen and M. H. Behfar, *Adv. Electron. Mater.*, 2023, **9**, 2201094.
15 L. Sokka, M. Välimäki, K. L. Väisänen, E. Hakola, M. Mäntysalo, J. Ollila, T. Happonen, L. Hakola and M. Smolander, *Flex. Print. Electron.*, 2024, **9**, 015007.
16 M. K. Välimäki, L. I. Sokka, H. B. Peltola, S. S. Ihme, T. M. J. Rokkonen, T. J. Kurkela, J. T. Ollila, A. T. Korhonen and J. T. Hast, *Int. J. Adv. Manuf. Technol.*, 2020, **111**, 325–339.
17 S. Khan, L. Lorenzelli and R. S. Dahiya, *IEEE Sens. J.*, 2015, **15**, 3164–3185.
18 L. Leonat, M. S. White, E. D. Głowacki, M. C. Scharber, T. Zillger, J. Rühling, A. Hübler and N. S. Sariciftci, *J. Phys. Chem. C*, 2014, **118**, 16813–16817.
19 M. Rawat, E. Jayaraman, S. Balasubramanian and S. S. K. Iyer, *Adv. Mater. Technol.*, 2019, **4**, 1–11.
20 F. Hoeng, A. Denneulin and J. Bras, *Nanoscale*, 2016, **8**, 13131–13154.

21 K. T. Huang, C. C. Chueh and W. C. Chen, *Mater. Today Sustain.*, 2021, **11–12**, 100057.
22 W. Li, Q. Liu, Y. Zhang, C. Li, Z. He, W. C. H. Choy, P. J. Low, P. Sonar and A. K. K. Kyaw, *Adv. Mater.*, 2020, **32**, 1–40.
23 M. Irimia-Vladu, E. D. Głowacki, G. Schwabegger, L. Leonat, H. Z. Akpinar, H. Sitter, S. Bauer and N. S. Sariciftci, *Green Chem.*, 2013, **15**, 1473–1476.
24 D. Angmo and F. C. Krebs, *J. Appl. Polym. Sci.*, 2013, **129**, 1–14.
25 I. Burgués-Ceballos, N. Kehagias, C. M. Sotomayor-Torres, M. Campoy-Quiles and P. D. Lacharmoise, *Sol. Energy Mater. Sol. Cells*, 2014, **127**, 50–57.
26 J. S. Goo, J. H. Lee, S. C. Shin, J. S. Park and J. W. Shim, *J. Mater. Chem. A*, 2018, **6**, 23464–23472.
27 K. D. Kim, T. Pfadler, E. Zimmermann, Y. Feng, J. A. Dorman, J. Wieckert and L. Schmidt-Mende, *APL Mater.*, 2015, **3**, 10.
28 L. V. Kayser and D. J. Lipomi, *Adv. Mater.*, 2019, **31**, 1–n.
29 J. Isaksson, P. Kjäll, D. Nilsson, N. Robinson, M. Berggren and A. Richter-Dahlfors, *Nat. Mater.*, 2007, **6**, 673–679.
30 M. Irimia-Vladu, E. D. Głowacki, G. Voss, S. Bauer and N. S. Sariciftci, *Mater. Today*, 2012, **15**, 340–346.
31 M. N. Nassajfar, I. Deviatkin, V. Leminen and M. Horttanainen, *Sustainability*, 2021, **13**, 12126.
32 H. Lissner, M. Wehrer, M. Reinicke, N. Horváth and K. U. Totsche, *Environ. Sci. Pollut. Res.*, 2015, **22**(4), 3158–3174.
33 G. Toscano, M. Colarieti, A. Anton, G. Greco and B. Biró, *Environ. Sci. Pollut. Res.*, 2014, **21**(15), 9028–9035.
34 E. B. Moustafa, S. S. Abdel Aziz, M. A. Taha and A. H. Saber, *Metals*, 2023, **13**, 836.
35 M. A. Zafar, Y. Liu and M. V. Jacob, *Chemosphere*, 2024, **362**, 142512.
36 S. Lee, Y. Hong and B. S. Shim, *Adv. Sustainable Syst.*, 2022, **6**, 1–9.
37 R. Saremi, N. Borodinov, A. M. Laradji and S. Sharma, *Molecules*, 2020, **25**, 3238.
38 A. Lamp, M. Kaltschmitt and J. Dethloff, *Molecules*, 2022, **27**, 466.
39 B. B. Tyussyupova, S. M. Tazhibayeva, K. Musabekov, Y. Mussatay and A. Kokanbaev, *Int. J. Eng. Res. Technol.*, 2020, **13**, 3699–3704.
40 J. Bonilla, R. B. Paiano, R. V. Lourenço, A. M. Q. B. Bittante and P. J. A. Sobral, *J. Polym. Environ.*, 2021, **29**, 1380–1395.
41 J. L. Smith and J. W. Doran, *Methods Assess. Soil Qual.*, 2015, **49**, 169–185.
42 B. M. Saalidong, S. A. Aram, S. Otu and P. O. Lartey, *PLoS One*, 2022, **17**, 1–17.